RSC Advances

PAPER

View Article Online
View Journal | View Issue

Cite this: *RSC Adv.*, 2016, **6**, 42288

Efficient fluoride adsorption by mesoporous hierarchical alumina microspheres†

Sara Gràcia Lanas,[a] Manuel Valiente,[b] Eleonora Aneggi,[a] Alessandro Trovarelli,[a] Marilena Tolazzi[a] and Andrea Melchior*[a]

Received 21st December 2015
Accepted 18th April 2016

DOI: 10.1039/c5ra27371d

www.rsc.org/advances

Mesoporous Hierarchical Alumina Microspheres (HAM) with high efficiency for fluoride removal have been synthesized and characterized. Two types of HAM, differing mostly in crystallinity, surface area and pore size have been obtained. Fluoride adsorption studies have been carried out by means of potentiometry and Isothermal Titration Calorimetry (ITC). The latter method has been applied for the first time to obtain direct determination of the adsorption enthalpy (ΔH_{ads}) of F^- ion on HAM. The kinetics of the reaction revealed a two-step process for fluoride adsorption on the adsorbent material. The ΔH_{ads} values obtained are clearly negative for the different samples investigated. Experimental adsorption data are well fitted by a Langmuir isotherm. The adsorption constant obtained for type A is 1 order of magnitude higher than for type B, showing that the synthetic protocol has a remarkable effect on this parameter. The highest defluoridation capacity reaches 26 mmol g^{-1} after 1 hour of equilibration for the amorphous HAM, which is higher than for other adsorbents reported in the literature.

Introduction

Groundwater contamination by fluoride is recognized as a serious problem worldwide, as fluoride can be toxic to humans in the case of chronic exposure to elevated concentrations.[1] Minerals containing fluoride are used by industries for several purposes such as glass and ceramic production, semiconductor manufacturing, brick and iron works, aluminum smelters and phosphate fertilizers.[1,2] Aside from natural geological fluoride enrichment of groundwater, anthropogenic contamination can elevate fluoride concentrations from ten to thousands of mg L^{-1}, much higher than the standard level recommended by the World Health Organization (1.5 mg L^{-1}).[1]

Fluoride absorbed by consumption of contaminated water is rapidly distributed through the body and integrated into the teeth and bones. The prolonged assumption of fluoride can cause several diseases, such as skeletal fluorosis.[1] Many health issues caused by fluoride consumption are irreversible,[3] thus it is necessary to control the fluoride concentration in drinking water.

The available water defluoridation methods include: adsorption,[3–12] precipitation,[13] electro-coagulation[14] or ion-exchange.[15] Among these technologies, adsorption seems to be most powerful method for fluoride removal from contaminated water, since it offers simplicity of plant design and lower energy and operative costs.[16]

Several materials have been tested for water defluoridation, for example alumina (Al_2O_3),[7,17] biosorbents,[18] clays[19] and composite materials.[20] However, most of fluoride sorption methods are unable to reach the concentration limit requested by international regulations (1.5 mg L^{-1})[1] thus, the optimization of materials for water defluoridation is still an actual challenge.

Alumina is recognized as one of the most effective materials for fluoride removal because of the high surface area and porosity, thermal stability and low solubility in a wide pH range.[21] For this application, several mesoporous alumina-based materials have been developed by modifying the original substrate and showed interesting defluoridation capacity.[6,9,22–24]

Hierarchically structured metal oxides have been recently employed in a wide range of applications from adsorption,[12,25,26] drug delivery,[27] catalysis,[28] to sensors[29] and electronic conversion and storage.[30] Among them, alumina-based hierarchical structures received a special attention due to its low cost and eco-friendly properties.[12]

The scope of this work is to study fluoride adsorption by high surface hierarchical alumina microspheres (HAM) and characterize the adsorption process in terms of loading capacity and thermodynamics.

HAM have been prepared and characterized by modification of standard methods, while adsorption studies have been carried out using a unique experimental approach, which combines potentiometry and Isothermal Titration Calorimetry (ITC).

[a]*Dipartimento Politecnico, Laboratori di Tecnologie Chimiche, Università di Udine, via del Cotonificio 108, 33100 Udine, Italy. E-mail: andrea.melchior@uniud.it*

[b]*Departamento de Quimica, Centre GTS, Universitat Autònoma de Barcelona, Campus Bellaterra Edificio CN, Barcelona, Spain*

† Electronic supplementary information (ESI) available. See DOI: 10.1039/c5ra27371d

In particular, ITC is an extremely powerful and high sensitive technique able to directly provide the heat evolved in a chemical process and then obtain useful information, such as stability constants and reaction enthalpy values. This technique has been hitherto widely used for the study of chemical equilibria in solution[31–35] and biomolecular interactions,[36] while only a limited number of examples of its application in adsorption studies can be found in the literature.[37–44]

Accurate data on the enthalpy associated to the adsorption process allow the design of the best conditions both for the uptake and for the eventual successive release of a given chemical species. In previous works, fluoride adsorption has been often modeled with Langmuir isotherm[5,7] and the associated enthalpy (ΔH_{ads}) has been calculated by the van't Hoff equation (using the temperature dependence of the Langmuir adsorption constant). However, many studies considered the discrepancies between enthalpy values obtained directly (ITC) and from van't Hoff equation and evidenced the large uncertainties associated to the latter method.[45–47] In this work, ITC is applied for the first time to obtain direct determination of ΔH_{ads} for fluoride ion adsorption by HAM to provide independent and more robust thermodynamic parameters.

Materials and methods

Synthesis of adsorbent material

Two types of HAM were synthesized using the methodology reported previously[48–50] with some modifications. All the reagents were of the analytical grade and used without any further purification. In a typical synthesis, a solution 0.05 M in aluminum sulfate and 0.1 M in urea was prepared in 100 mL of distilled water and then stirred thoroughly during 15 minutes. Then 35 mL of the prepared solution were added in a Teflon-lined digestion vessel of 100 mL capacity and then placed on a turntable for uniform heating using a microwave digestion system. The microwave treatment was conducted in a temperature-controlled mode at 180 °C by non-pulse heating time for 3 min (type A) or 20 min (type B), using 2.45 GHz microwave radiation under power range of 0–1000 W (using maximum power). Afterwards the sample was left for cooling until ambient temperature was reached. The pH of the resultant solution was adjusted at ~9 with NaOH. The synthesized material was then collected by centrifugation and washed with hot distilled water and ethanol several times. The precipitate was dried in an oven at 80 °C for 12 h. In order to convert the resulting γ-AlOOH obtained in this synthesis into Al_2O_3, the powder was calcinated in a muffle furnace at 600 °C for 2 hours.

Material characterization

The particles were analyzed by transmission electron microscopy (TEM) using a Transmission Electronic Microscope JEM-2011, resolution: 0.18 nm at 200 kV, accelerating voltage: 80–200 kV, equipped with camera: CCD GATAN 895 USC 4000, detector EDS Oxford LINCA with energy resolution: 136 eV. Scanning electron microscopy (SEM) analyses were performed by MERLIN FE-SEM, ZEISS with the detector EDS Oxford LINCA X-Max and EBSD analysis Oxford Nordlys II.

Textural characteristics of all fresh samples were measured according to the Brunauer–Emmett–Teller (BET) equation by nitrogen adsorption isotherms at −196 °C. Pore size distributions were calculated by applying the Barrett–Joyner–Halenda (BJH) method to the isotherms desorption branch. These measurements were carried out in a Tristar 3000 gas adsorption analyzer (Micromeritics). Prior to the adsorption measurements, the samples were degassed at 150 °C during 1 h.

The particle size distribution was determined by dynamic light scattering (DLS) on a Horiba LB-550 Particle Size Analyzer. Around 5 mg of HAM A and B respectively were suspended in 10 mL of TISAB solution. The suspensions were sonicated during 15 min previously to the DLS measurement.

X-ray powder diffraction (XRD) patterns were determined using a Philips PW3040/60 PRO instrument (equipped with an x'celerator detector) operating at 40 kV and 40 mA with Ni-filtered Cu K_α radiation. Diffraction profiles were collected in the 2θ range of 5–100 °C with a step of 0.02 and counting time of 15 s per step.

The pH value of zero point charge (pH_{zpc}) was determined by solid addition method[2] using 0.1 M potassium chloride (KCl) solution with 20 mg L^{-1} F^-. 20 mL of the prepared solution (0.1 M KCl with fluoride) were added into a series of vessels. Then, the initial pH (pH_i) of the solutions was adjusted in the range of 3.0–10.0. After that, 15 mL of any solution were added into another vessel with 0.3 mg of the adsorbent material. The suspensions were then equilibrated for 48 h.

Once the equilibration time was reached, the final pH (pH_f) of the solutions was measured again. The difference between the final and the initial pH ($\Delta pH = pH_i - pH_f$) was plotted *versus* the pH_i. The point of zero charge is given for the point where the curve intersect with abscissa, at this point $\Delta pH = 0$. In order to confirm our results, the experiment was performed at different ionic strength, 0.1 M and 0.01 M KCl.

Potentiometry

Potentiometric studies for fluoride removal were performed adding 20 mL of 0.5 g L^{-1} HAM suspension into a vessel and then titrating with sodium fluoride (NaF) solution 80 mM. 0.5 mL of fluoride solution was added to the suspension and once the equilibrium time was expired (1 h), the fluoride concentration in solution was measured using a fluoride selective electrode (Really-Flow™ Solid-State combination fluoride-selective Electrode, Weiss Research) before the consecutive addition. The suspension was kept under stirring during the experiment and in total around 9–13 equal-volume additions were made for each experiment.

The experiments were performed in total ionic strength adjustment buffer (TISAB), which was prepared following the procedure described.[51] At the pH fixed by TISAB solution, the formation of hydrofluoric acid (HF) is negligible and the concentration of hydroxyls (OH^-), the only other anion that the electrode responds to, is insignificant.

Potentiometric data have been fitted both with Langmuir and Freundlich isotherms at different temperatures (298.15 and 318.15 K).[5–8,52] The Langmuir isotherm describes an

homogeneous sorption, where all active sites have equal affinity for the adsorbate, and makes possible to obtain the value of the adsorption constant (b) and loading capacity (Q_{max}) of the HAM[53,54] according to the equation:

$$[F^-]_{ads} = \frac{Q_{max} b [F^-]_e}{1 + b[F^-]_e} \quad (1)$$

where: $[F^-]_e$ = equilibrium fluoride concentration (M), $[F^-]_{ads}$ = fluoride adsorbed at equilibrium (mol g^{-1}), Q_{max} = maximum quantity of adsorbed F^- per gram of HAM (mol g^{-1}) and b = Langmuir constant (M^{-1}).

Freundlich isotherm specifies the adsorption for heterogeneous surfaces characterized by the heterogeneity factor $1/n$ represented by equation:

$$[F^-]_{ads} = K_f [F^-]_e^{\frac{1}{n}} \quad (2)$$

K_f is the Freundlich constant ((L $mmol^{-1}$ $g^{-1})^{1/n}$).

Additional batch titrations were performed for sample A only. In a typical experiment, 20 mL of fluoride solutions with different initial concentrations (0.5–16 mM) were mixed with 10 mg of HAM for a specified contact time (1 h) at 298.15 K. After the equilibrium, fluoride concentration was then measured using the fluoride selective electrode.

Isothermal titration calorimetry

Fluoride samples and the standard solutions for calorimetric studies were also prepared in TISAB buffer. ITC experiments have been carried out at 298.15 K using a TAMIII thermostat (TA Instruments) equipped with a nanocalorimeter (1 mL cell volume) and an automatic titration syringe. The sample was stirred continuously at 90 rpm and the reference cell was filled with 0.8 mL of distilled water throughout all experiments.

In a typical experiment, about 10 additions of 17.5 μl of 80 mM fluoride solution were added to 0.7 mL of ~0.5 g L^{-1} HAM suspension. The delay time between two consecutive injections was set to 60 min, which was long enough to let the system to reach thermal equilibrium.

The values of b and Q_{max} calculated with Langmuir isotherm from potentiometric data have been used to calculate $[F^-]_e$ for each titrant addition by numerically solving eqn (1) in the experimental conditions of the calorimetric titrations. The ΔH_{ads} (kJ mol^{-1}) value has been calculated to best fit the experimental heat for the fluoride adsorption according to the modified isotherm[42] shown below:

$$q_{cum} = \frac{Q_{max} b [F^-]_e}{1 + b[F^-]_e} \Delta H_{ads} \quad (3)$$

where: q_{cum} = total heat involved in the reaction per gram of adsorbent (kJ g^{-1}). Dilution heat (q_{dil}) was also determined to correct the total heat measured (q_{meas}) by the instrument. Thereby $q_{cum} = q_{meas} - q_{dil}$, represents only the heat involved on the adsorption reaction. Data analysis has been done within the MS-Excel using Solverstat and EST utilities.[55,56]

Results and discussion

Characterization of the adsorbent material

The SEM and TEM micrographs obtained for the two samples (type A and B) do not reveal significative difference. The SEM images in Fig. 1A-i and B-i reveal flower-like hollow microspheres with a highly textured surface and smooth inner wall surface. The microspheres have a diameter of ~0.9 μm, which is significantly smaller than those obtained by the published methodology (5 μm).[48] In Fig. 1A-ii and B-ii TEM images show a magnification of the particles, where the detailed morphology of the flower-like microspheres (consisting in a randomly assembly of nanoplatelets) can be seen. The detailed TEM images given in Fig. 1A-iii and B-iii, evidence the hierarchical structure of the particles formed by the packing of nanoplatelets about 200 nm length and thin thickness. In Fig. 1A-iv and B-iv an enlargement of the nanoplatelets evidencing the smooth surface is also shown.

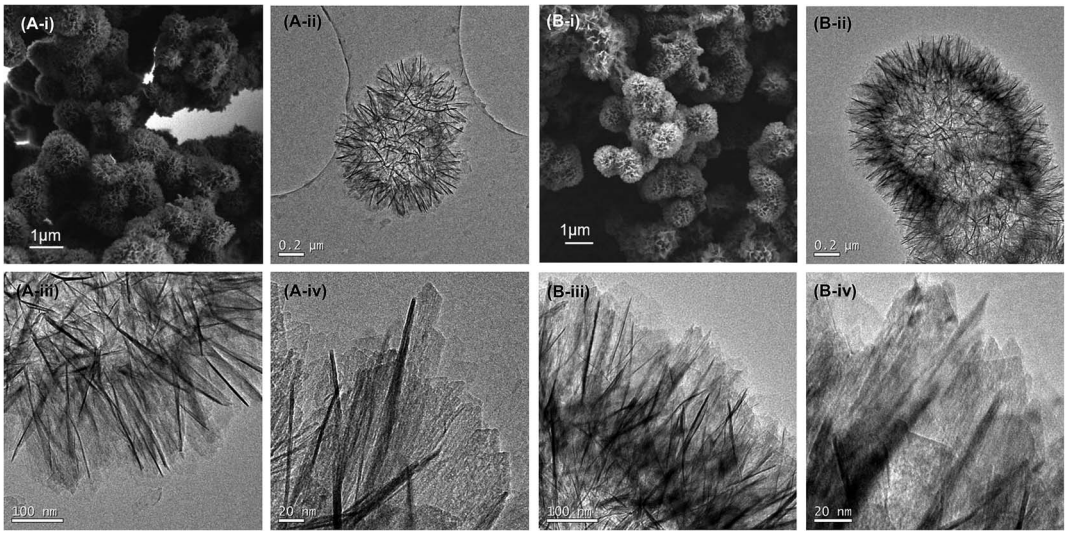

Fig. 1 SEM (A-i and B-i) and TEM (A-ii, A-iii, A-iv, B-ii, B-iii and B-iv) images of synthesized HAM of type A and B.

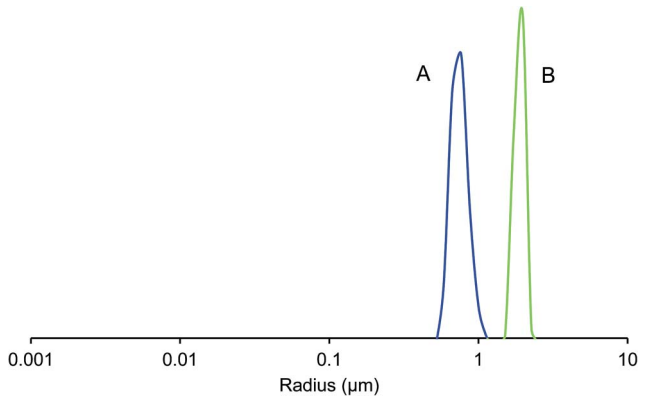

Fig. 2 Particle size distribution of HAM for type A (blue) and B (green) determined by DLS (suspension in TISAB).

In Fig. S1 (ESI†) representative SEM and TEM images of the uncalcined type B HAM are reported. It can be seen that the microspheres have the same characteristic structure of the calcined HAM, indicating that the hierarchical morphology is stable, even after high temperature treatment.

The particle size distribution of the two samples analyzed by DLS is represented in Fig. 2. In Fig. 2A it can be seen that the HAM suspension of type A was obtained with an average diameter between 0.6 and 1 μm. This value corresponds approximately with the diameter of the particles, which means that the particles aggregation is almost absent in our working conditions. The distribution of type B is shown in Fig. 2B, which indicates an average size larger than type A.

The adsorption–desorption isotherms (Fig. 3) can be classified as Type IV,[57] characteristic of mesoporous materials.[57] The H3 type-hysteresis loop[58] at high relative pressures (over pressure P/P_o of 0.7 in both types A and B) indicates the presence of mesoporous formed between the assembly of the nanoplatelets.[59] The BET surface area of the synthesized material was found to be 254.1 $m^2\ g^{-1}$ and 241.6 $m^2\ g^{-1}$ for type A and B respectively. A mesoporous material normally contains pores with diameters between 2 and 50 nm. The BJH pore size was determined to be 12.96 nm with a pore volume of 1.07 $cm^3\ g^{-1}$ for sample A and 25.55 nm and 2.32 $cm^3\ g^{-1}$ for sample B, which confirms the mesoporosity of our material. Because of the characteristic downy surface of the particles, the synthesized alumina has excellent porous properties and seems to exhibit a great potential for fluoride adsorption.

No clear peaks were observed in the diffractogram of type A (Fig. 4), indicating that the HAM are amorphous while the microspheres of type B showed some characteristic peaks for aluminum oxide in accordance with Al_2O_3 reference standard diffractogram (JCDPS card no. 10-0425). However, the low intensity of the signals evidenced that the material is a poorly crystalline solid.

It has been previously suggested that the crystallinity of alumina based adsorbents to have an influence on the fluoride adsorption capacity[60] and that low crystallinity of alumina-based materials seems to be an advantage for their adsorption capacity.[12,60–62] According to these observations, type A, in principle, would be the most efficient material for a fluoride adsorption.

The point of zero charge for both type A and B is $pH_{zpc} = 9.0$ at different ionic strength (0.1 M and 0.01 M KCl). At the working pH = 5.5, the surface of the alumina is positively charged, therefore the interaction of alumina surface with the solution containing F^- could be represented by the following reactions:[3,8,51]

$$\equiv AlOH + H^+ \leftrightarrow \equiv AlOH_2^+ \quad (4)$$

$$\equiv AlOH_2^+ + F^- \leftrightarrow \equiv AlF + H_2O \quad (5)$$

The physical features of samples A and B are summarized in Table S1.†

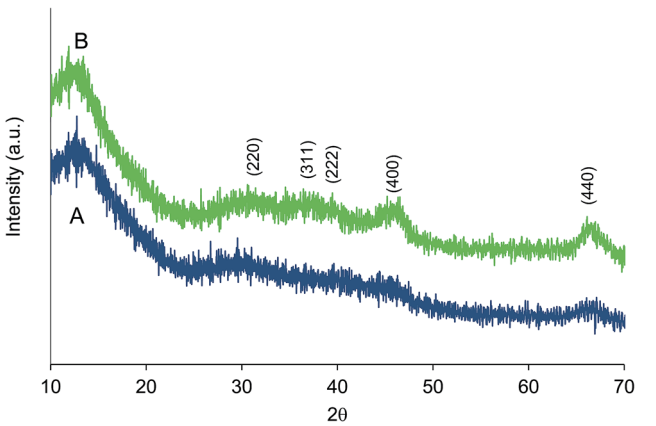

Fig. 4 X-ray diffraction (XRD) patterns of HAM for type A (blue) and B (green) samples.

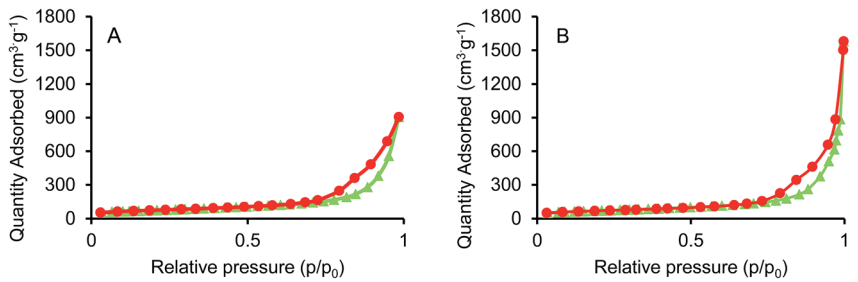

Fig. 3 N_2 adsorption (green triangles) and desorption (red circles) isotherms of HAM for type A (Fig. 2A) and sample B (Fig. 2B).

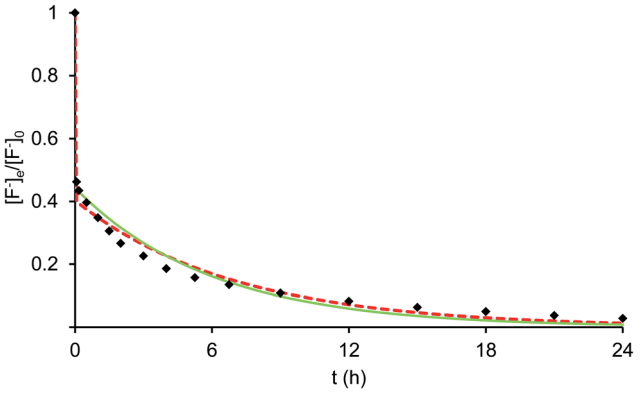

Fig. 5 Fluoride adsorption kinetics on HAM (type A, 0.5 g L^{-1}, pH = 5.5, T = 298.15 K, $[F^-]_0$ = 16 mM) fitted with mono- (green line) and bi- (dashed red line) exponential functions.

Fluoride adsorption

In Fig. 5 the $[F^-]_e/[F^-]_0$ ratio *vs.* time (h) plot for an adsorbent dose of 0.5 g L^{-1} and initial concentration of 16 mM of fluoride is shown (type A). Experimental data were fitted with both mono and bi-exponential eqn (6) and (7):

$$[F^-]_e = a_1 e^{-k_1 t} \quad (6)$$

$$[F^-]_e = a_1 e^{-k_1 t} + a_2 e^{-k_2 t} \quad (7)$$

The fitting results obtained are summarized in Table S3† in the ESI.† The bi-exponential model better fits the experimental data with respect to the mono-exponential and suggests the presence of a fast first reaction followed by a much slower process (k_2 is 3 orders of magnitude lower than k_1, Table S3†). This has also been observed for fluoride absorption by MgAl–CO_3 layered double hydroxides.[63] The fast adsorption step occurs during the first hour, then the rate decreases and, after 3 h, 75% of the initial fluoride is removed.‡

In Fig. 6, the heat evolved for each addition of fluoride to HAM suspension (for type A and B) is shown. The heat signal reaches the baseline in 60 minutes that is, the heat exchanged related to the F^- adsorption on the HAM expires in 1 hour. Although the equilibrium is not yet reached according to the overall reaction model (Fig. 5), in ITC experiments it seems that only the first process produces a detectable thermal effect. Therefore, calorimetric experiments were analyzed by using $[F^-]_e$ values calculated from potentiometric data with the same delay time between additions (60 min) as in calorimetry (Table 1).

Potentiometric data for fluoride adsorption by HAM (type A and B) were fitted both with the Langmuir and Freundlich isotherms (Fig. 7) and the resulting parameters are reported in Table 1. Potentiometric batch titrations carried out for type A sample confirmed the values obtained (Fig. S2 and Table S2 in the ESI†).

‡ a_i = initial concentration for each exponential (M), k_i = constant rates (h^{-1}), t = time (h).

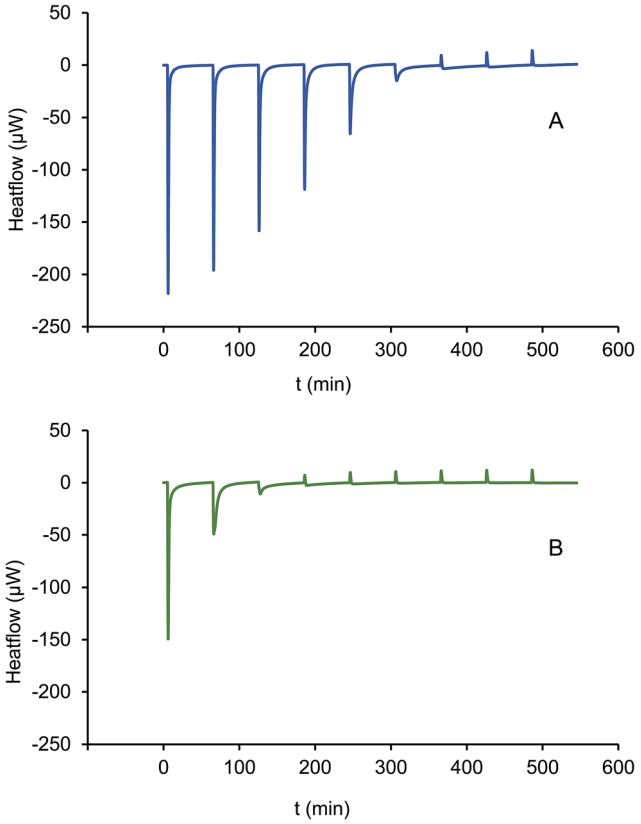

Fig. 6 ITC for fluoride adsorption into HAM of type A (blue) and type B (green). Each peak corresponds to an injection of 17.5 μl of 80 mM fluoride solution to 0.7 mL of 0.5 g L^{-1} HAM suspension.

Experimental points are better represented by the Langmuir than the Freundlich model suggesting the presence of a homogeneous anion adsorption, forming a monolayer on the positively charged surface of the microspheres. The Langmuir constant obtained for type A is significantly higher than for type B (~1 order of magnitude, Table 1) showing that the synthetic protocol has a remarkable effect on this parameter. While the difference in the BET surface areas of both samples is not remarkable, DLS experiments evidenced higher particle aggregation in type B (Fig. 2 and Table S1†). However, the higher efficiency in fluoride removal for type A than type B seems also to be related to the different crystallinity of the two samples, as previously found.[12,60–62]

The maximum loading capacity of the material (Q_{max}) results higher for sample A than sample B, being 0.026 and 0.020 moles of fluoride per gram of material, respectively. These values are higher than those found for other alumina-based adsorbents which are reported in Table 2[2,3,5–7,9–12,64–67] and for other adsorbent materials reported in Table S4 in the ESI.†[20,68–72]

The high efficiency of the HAM could be associated to the structure of the hierarchical material. As suggested,[70] the mesoporosity and the elevated surface area gives to the material a high number of active sites exposed to the surface. In addition, the particularity of the hierarchical materials avoids the aggregation of the nanoplatelets, exposing their entire surface to adsorb F^-.[70]

Table 1 Langmuir and Freundlich isotherm parameters for fluoride adsorption by HAM of type A and B with different experimental conditions

			Langmuir equation					Freundlich equation		
Type	Temperature (K)	Delay time (h)	Q_{max} (mol g^{-1})	b (M^{-1})	log b	R^2	n	K_f (L mmol^{-1} g^{-1})	log K_f	R^2
A	318.15	1	0.039 ± 0.002	4165 ± 794	3.62 ± 0.19	0.961	3.1 ± 0.5	31 ± 1	1.49 ± 0.03	0.721
A	298.15	1	0.026 ± 0.001	4563 ± 486	3.66 ± 0.11	0.979	5.9 ± 0.5	20.2 ± 0.3	1.31 ± 0.01	0.871
A	298.15	12	0.055 ± 0.001	4820 ± 394	3.68 ± 0.08	0.999	4.4 ± 0.6	42 ± 1	1.62 ± 0.02	0.847
B	298.15	1	0.020 ± 0.001	598 ± 100	2.78 ± 0.17	0.967	2.3 ± 0.1	7.6 ± 0.3	0.88 ± 0.04	0.895

Similar potentiometric experiments with 12 h delay between additions have been also performed (type A) to study the adsorption of fluoride at long times (Fig. S3†). The resulting adsorption constant is quite similar to that obtained with a 1 h delay, while the loading capacity is ~50% larger.

The experimental and calculated q_{cum} values for type A and B are shown in Fig. 8. In type B, after the third injection the heat flow measured for the remaining injections corresponds to the dilution heat indicating that the adsorption process is finished, while for type A 6 injections are needed. It is also evidenced that the total heat evolved in fluoride adsorption in type A is significantly higher than in type B, which confirms that type A is a more efficient adsorbent for fluoride removal than type B.

The process is clearly exothermic for both type A and B samples (Table 2) and, as can be observed, the adsorption enthalpy obtained for type B ($\Delta H_{ads} = -13.3 \pm 0.9$ kJ mol^{-1}) is less negative than the value obtained for type A ($\Delta H_{ads=} -17.7 \pm 0.6$ kJ mol^{-1}). The ΔH_{ads} values obtained previously by van't Hoff equation are in most cases positive[2,5,7] and spread over a wide range (6.8–36.6 kJ mol^{-1}). Nevertheless, also negative ΔH_{ads} have been reported for other alumina-based adsorbents,[3,64] natroalunite microtubes,[11] nanosized iron oxides[68] or UiO-66-NH$_2$ [72] (values ranging from −0.8 to −94.7 kJ mol^{-1}, Table 2 and S4†).

To compare our method for the determination of ΔH_{ads} with the standard van't Hoff interpolation, normally used in previous works,[2,3,5,7,11,20,64,68,72] the adsorption parameters were determined for HAM (type A) also at 318 K (Table 1).

The ΔH_{ads} value calculated by the van't Hoff equation ($\Delta H_{ads} \sim -4$ kJ mol^{-1}), is less negative than that obtained by ITC measurements. However, when ΔH_{ads} is calculated with the van't Hoff equation, the propagated uncertainty on the ΔH_{ads} values can be large. Thus, an ideal ΔH_{ads} determined by van't Hoff equation should be calculated using very precise values of equilibrium constants and in a large range of temperature where, on the other hand, the heat capacity is not rigorously constant. Therefore, the direct determination of the heat exchanged by ITC seems to be the sole way to obtain reliable heats of adsorption and calculate ΔH_{ads} values.

It can be noticed that the $T\Delta S_{ads}$ terms (obtained from the ΔG_{ads} calculated with the b values at 298.15 K in Table 1 and the ΔH_{ads} values in Table 2) are nearly the same for the two materials (+3.2 and +2.6 kJ mol^{-1} for HAM A and B respectively). This positive entropy change is in agreement with previous results adsorption of metal cations[39,43] and reflects the increase disorder due to charge neutralization and desolvation of the fluoride anion.

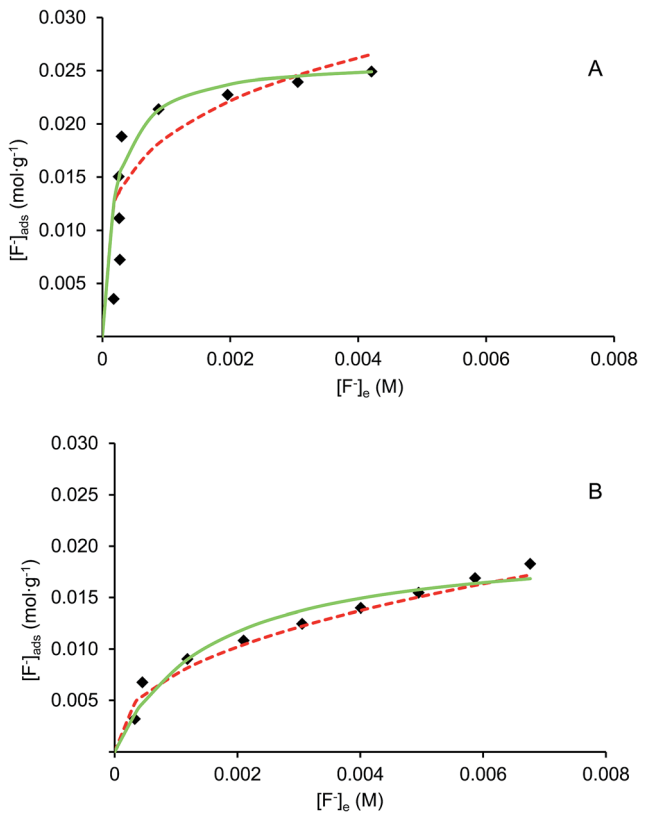

Fig. 7 Experimental fluoride adsorption isotherms presenting the experimental data fitted with Langmuir (green line) and Freundlich (dashed red line) models with 1 h between injections for type A and B.

Conclusions

In this work, two new HAM adsorbents have been synthesized and used for fluoride removal. SEM, TEM, BET and XRD diffraction studies reveal a high porous structure of amorphous alumina. The two types show similar physical characteristics with small differences in pore size and specific surface area. The main difference between the two samples is the presence of crystalline phase, smaller pore size and higher surface area in the one prepared with a shorter microwave treatment (type A). The kinetic study reveals a bi-exponential model indicating a two-step process for fluoride adsorption.

Fluoride adsorption experiments evidenced that the amorphous HAM (type A) have a superior affinity for F^- ion than type

Table 2 Fluoride removal parameters for several alumina-based adsorbents. In parentheses the original values reported in the references

Adsorbent	Particle size	Initial F^- (mM)	Adsorbent dosage (g L^{-1})	pH	T (K)	Contact time (h)	Adsorption capacity (mmol g^{-1})	b (M^{-1})	ΔH (kJ mol^{-1})	Ref.
Nano alumina	—	0.05–5.3 (1–100 mg L^{-1})	1.0	6.15	298	24	0.8 (15.43 mg g^{-1})	3240	14.8	2
Aluminum hydroxide	—	—	0.5	4	303	2	3.4 (63.5 mg g^{-1})	623.7 (0.033 L mg^{-1})	−18.45	3
Fe_3O_4@$Al(OH)_3$	240–340 nm	0–8.5 (0–160 mg L^{-1})	1.0	6.5	298	1	4.7 (88.48 mg g^{-1})	5557 (0.2 L mg^{-1})	6.8	5
Mesoporous calcium-doped alumina	—	0.1–52.9 (2–1000 mg L−1)	0.1	6.5	298	12	23.8 (450 mg g^{-1})	—	—	6
Al_2O_3	12–15 μm	0.5–7.9 (10–150 mg L^{-1})	1.0	6	298	48	4.4 (83.33 mg g^{-1})	37 800 (2.000 L mg^{-1})	36.66	7
Ordered mesoporous alumina	300–800 nm	0.3–10.6 (5–200 mg L^{-1})	0.5	6	298	12	7.1 (135 mg g^{-1})	13 854 (0.733 L mg^{-1})	—	9
Heated nano-gibbsite	—	0.263–3.947	2.0	6.0	4	4	1.6 (30.55 mg g^{-1})	0.272	—	10
Natroalunite microtubes	—	0.3–10.6 (5–200 mg L^{-1})	1.0	7.0	298	24	4.5 (85.84 mg g^{-1})	3.750	−30.80	11
Amorphous aluminum oxide microspheres	—	0.3–7.9 (5–150 mg L^{-1})	0.5	7.0	298	—	6.7 (126.90 mg g^{-1})	7938 (0.42 L mg^{-1})	—	12
Chitosan based mesoporous alumina	—	—	2.0	6.8	303	24	0.4 (8.264 mg g^{-1})	2319 (0.1227 L mg^{-1})	−0.8	64
Tea-APAM-Al	—	0.3–10.6 (5–200 mg L^{-1})	1.0	5.0	308	3	2.2 (42.14 mg g^{-1})	1767.1 (0.09350 L mg^{-1})	—	65
Tea-Al-Fe	—	0.5–10.5 (10–200 mg L^{-1})	2.0	7.0	298	2	1.0 (18.52 mg g^{-1})	1051.9 (0.05537 L mg^{-1})	—	66
Al_2O_3–ZrO_2	—	2.6–7.9 (50–150 mg L^{-1})	1.0	2.0	318	4	6.0 (114.54 mg g^{-1})	228.0 (0.012 L mg^{-1})	−2.414	67
HAM type A	900 nm	2.0–16.0	0.5	5.5	298.15	12[a]	55.0 (1.0 g g^{-1})	4820	—	Present work
HAM type A	900 nm	2.0–16.0	0.5	5.5	298.15	1[a]	26.0 (491.4 mg g^{-1})	4563	−17.7 ± 0.6	Present work
HAM type B	900 nm	2.0–16.0	0.5	5.5	298.15	1[a]	20.4 (385.6 mg g^{-1})	598	−13.3 ± 0.9	Present work

[a] Delay time between fluoride solution additions.

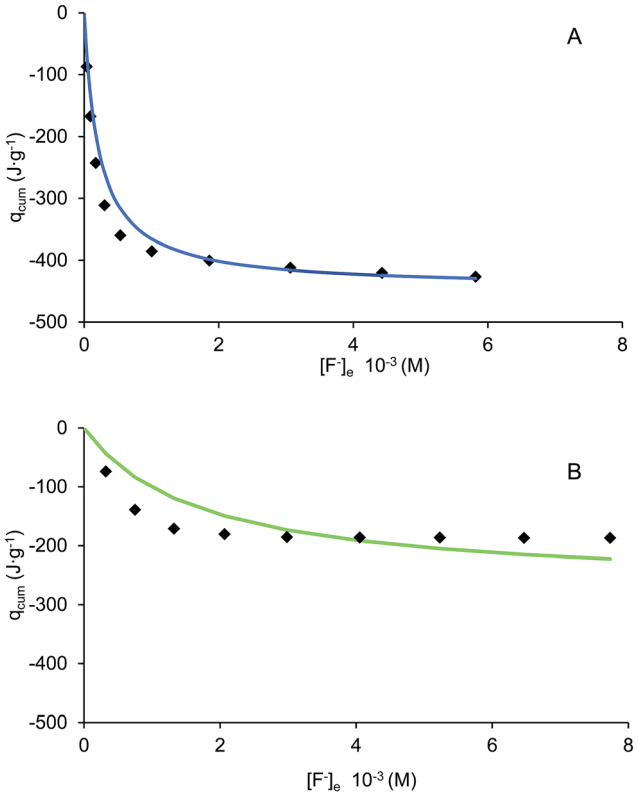

Fig. 8 Experimental calorimetric data fitted with calorimetric Langmuir isotherm (line) for type A (blue) and B (green) HAM.

B, being the Langmuir constant about 1 order of magnitude higher. Adsorption experiments have shown that synthesized materials have a high efficiency towards defluoridation, with a maximum loading capacity of 0.026 moles of fluoride per gram of material after 1 h contact time, which is significantly better than most other materials reported in the literature. Therefore our results show that the synthesized HAM have high defluoridation capacity, which makes them a potential candidate for water treatment.

The combined potentiometric-ITC method has been used to calculate the adsorption parameters and, for the first time, to obtain the ΔH_{ads} value by direct measurement of the heat associated to the process. Contrarily to the data presented in most previous works, clearly negative enthalpy values for fluoride adsorption are obtained here. Therefore, ITC can be a useful tool for an accurate and relatively fast screening of sorbent materials.

Acknowledgements

The present work has been partially supported by the Spanish MINECO grant CTM2012-30970.

References

1 Environmental Health Criteria, Fluorides, World Health Organization (WHO), Geneva, 2002.
2 E. Kumar, A. Bhatnagar, U. Kumar and M. Sillanpää, *J. Hazard. Mater.*, 2011, **186**, 1042–1049.
3 M. G. Sujana, G. Soma, N. Vasumathi and S. Anand, *J. Fluorine Chem.*, 2009, **130**, 749–754.
4 B. D. Turner, P. Binning and S. L. S. Stipp, *Environ. Sci. Technol.*, 2005, **39**, 9561–9568.
5 X. Zhao, J. Wang, F. Wu, T. Wang, Y. Cai, Y. Shi and G. Jiang, *J. Hazard. Mater.*, 2010, **173**, 102–109.
6 W. Li, C. Y. Cao, L. Y. Wu, M. F. Ge and W. G. Song, *J. Hazard. Mater.*, 2011, **198**, 143–150.
7 W. X. Gong, J. H. Qu, R. P. Liu and H. C. Lan, *Chem. Eng. J.*, 2012, **189–190**, 126–133.
8 L. Chai, Y. Wang, N. Zhao, W. Yang and X. You, *Water Res.*, 2013, **47**, 4040–4049.
9 C. Yang, L. Gao, Y. Wang, X. Tian and S. Komarneni, *Microporous Mesoporous Mater.*, 2014, **197**, 156–163.
10 M. Vithanage, A. U. Rajapaksha, M. S. Bootharaju and T. Pradeep, *Colloids Surf., A*, 2014, **462**, 124–130.
11 B.-S. Zhu, Y. Jia, Z. Jin, B. Sun, T. Luo, X.-Y. Yu, L.-T. Kong, X.-J. Huang and J.-H. Liu, *Chem. Eng. J.*, 2015, **271**, 240–251.
12 D. Kang, S. Tong, X. Yu and M. Ge, *RSC Adv.*, 2015, **5**, 19159–19165.
13 D. Thakre, S. Jagtap, A. Bansiwal, N. Labhsetwar and S. Rayalu, *J. Fluorine Chem.*, 2010, **131**, 373–377.
14 M. Bennajah, B. Gourich, A. H. Essadki, C. Vial and H. Delmas, *Chem. Eng. J.*, 2009, **148**, 122–131.
15 N. Chubar, *J. Colloid Interface Sci.*, 2011, **357**, 198–209.
16 L. H. Velazquez-Jimenez, E. Vences-Alvarez, J. L. Flores-Arciniega, H. Flores-Zuñiga and J. R. Rangel-Mendez, *Sep. Purif. Technol.*, 2015, **150**, 292–307.
17 J. Chilton, E. Dahi, M. Lennon and P. Jackson, *Fluoride in Drinking-water*, World Health Organization (WHO), Geneva, 2006.
18 V. Tomar, S. Prasad and D. Kumar, *Microchem. J.*, 2014, **112**, 97–103.
19 N. Hamdi and E. Srasra, *Desalination*, 2007, **206**, 238–244.
20 S. Wen, Y. Wang and S. Dong, *RSC Adv.*, 2015, **5**, 89594–89602.
21 Y. Kim, C. Kim, I. Choi, S. Rengaraj and J. Yi, *Environ. Sci. Technol.*, 2004, **38**, 924–931.
22 Y. Q. He, N. N. Zhang and X. D. Wang, *Chin. Chem. Lett.*, 2011, **22**, 859–862.
23 J. Han, Z. Du, W. Zou, H. Li and C. Zhang, *Chem. Eng. J.*, 2015, **262**, 571–578.
24 M. Nazari and R. Halladj, *J. Taiwan Inst. Chem. Eng.*, 2014, **45**, 2518–2525.
25 J. Zhang, S. Liu, J. Lin, H. Song, J. Luo, E. M. Elssfah, E. Ammar, Y. Huang, X. Ding, J. Gao, S. Qi and C. Tang, *J. Phys. Chem. B*, 2006, **110**, 14249–14252.
26 W. Cai, J. Yu and M. Jaroniec, *J. Mater. Chem.*, 2010, **20**, 4587.
27 W. Wei, G. Hu, D. Yu, T. Mcleish, Z. Su and Z. Shen, *J. Am. Chem. Soc.*, 2008, **130**, 15808–15810.
28 H. Guo, Y. He, Y. Wang, L. Liu, X. Yang, S. Wang, Z. Huang and Q. Wei, *J. Mater. Chem. A*, 2013, **1**, 7494–7499.
29 C. Peng, J. Guo, W. Yang, C. Shi, M. Liu, Y. Zheng, J. Xu, P. Chen, T. Huang and Y. Yang, *J. Alloys Compd.*, 2016, **654**, 371–378.

30 P. Yu, X. Zhang, D. Wang, L. Wang and Y. Ma, *Cryst. Growth Des.*, 2009, **2008**, 528–533.
31 L. Cavallo, S. Del Piero, J.-M. Ducéré, R. Fedele, A. Melchior, G. Morini, F. Piemontesi and M. Tolazzi, *J. Phys. Chem. C*, 2007, **111**, 4412–4419.
32 F. Endrizzi, A. Melchior, M. Tolazzi and L. Rao, *Dalton Trans.*, 2015, **44**, 13835–13844.
33 A. Melchior, E. Peralta, M. Valiente, C. Tavagnacco, F. Endrizzi and M. Tolazzi, *Dalton Trans.*, 2013, **42**, 6074–6082.
34 P. Di Bernardo, P. L. Zanonato, A. Melchior, R. Portanova, M. Tolazzi, G. R. Choppin and Z. Wang, *Inorg. Chem.*, 2008, **47**, 1155–1164.
35 P. Di Bernardo, P. L. Zanonato, F. Benetollo, A. Melchior, M. Tolazzi and L. Rao, *Inorg. Chem.*, 2012, **51**, 9045–9055.
36 J. E. Ladbury and M. L. Doyle, *Biocalorimetry 2: Applications of Calorimetry in the Biological Sciences*, Wiley, Chichester, 2004.
37 M. E. Strayer, J. M. Binz, M. Tanase, S. M. Kamali Shahri, R. Sharma, R. M. Rioux and T. E. Mallouk, *J. Am. Chem. Soc.*, 2014, **136**, 5687–5696.
38 L. N. H. Arakaki, M. G. da Fonseca, E. C. da Silva Filho, A. P. D. M. Alves, K. S. de Sousa and A. L. P. Silva, *Thermochim. Acta*, 2006, **450**, 12–15.
39 L. N. H. Arakaki, V. L. S. A. Filha, A. F. S. Germano, S. S. G. Santos, M. G. Fonseca, K. S. Sousa, J. G. P. Espínola and T. Arakaki, *Thermochim. Acta*, 2013, **556**, 34–40.
40 N. Welsch, Y. Lu, J. Dzubiella and M. Ballauff, *Polymer*, 2013, **54**, 2835–2849.
41 P. R. S. Braga, A. A. Costa, J. L. de Macedo, G. F. Ghesti, M. P. de Souza, J. A. Dias and S. C. L. Dias, *Microporous Mesoporous Mater.*, 2011, **139**, 74–80.
42 C. W. Chronister and R. S. Drago, *J. Am. Chem. Soc.*, 1993, **115**, 4793–4798.
43 R. S. Drago, S. C. Dias, M. Torrealba and L. de Lima, *J. Am. Chem. Soc.*, 1997, **119**, 4444–4452.
44 W. Lin, J. Walter, A. Burger, H. Maid, A. Hirsch, W. Peukert and D. Segets, *Chem. Mater.*, 2015, **27**, 358–369.
45 Y. Liu and J. M. Sturtevant, *Protein Sci.*, 1995, **4**, 2559–2561.
46 Y. Liu and J. M. Sturtevant, *Biophys. Chem.*, 1997, **64**, 121–126.
47 L. S. Mizoue and J. Tellinghuisen, *Biophys. Chem.*, 2004, **110**, 15–24.
48 W. Cai, J. Yu and S. Mann, *Microporous Mesoporous Mater.*, 2009, **122**, 42–47.
49 X. Wu, B. Zhang and Z. Hu, *Mater. Lett.*, 2012, **73**, 169–171.
50 X. Wu, B. Zhang and Z. Hu, *Mater. Lett.*, 2013, **91**, 249–251.
51 S. S. Tripathy, J. L. Bersillon and K. Gopal, *Sep. Purif. Technol.*, 2006, **50**, 310–317.
52 S. G. Wang, Y. Ma, Y. J. Shi and W. X. Gong, *J. Chem. Technol. Biotechnol.*, 2009, **84**, 1043–1050.
53 G. Limousin, J. P. Gaudet, L. Charlet, S. Szenknect, V. Barthès and M. Krimissa, *Appl. Geochem.*, 2007, **22**, 249–275.
54 K. Y. Foo and B. H. Hameed, *Chem. Eng. J.*, 2010, **156**, 2–10.
55 C. Comuzzi, P. Polese, A. Melchior, R. Portanova and M. Tolazzi, *Talanta*, 2003, **59**, 67–80.
56 S. del Piero, A. Melchior, P. Polese, R. Portanova and M. Tolazzi, *Ann. Chim.*, 2006, **96**, 29–49.
57 S. Lowell, J. E. Shields, M. A. Thomas and M. Thommes, *Characterization of Porous Solids and Powders: Surface Area, Pore Size and Density*, Kluwer Academic Publishers, Dordrecht, 2004.
58 K. S. W. Sing and R. T. Williams, *Adsorpt. Sci. Technol.*, 2004, **22**, 773–782.
59 W. Cai, J. Yu, S. Gu and M. Jaroniec, *Cryst. Growth Des.*, 2010, **10**, 3977–3982.
60 J. Du, D. A. Sabatini and E. C. Butler, *Chemosphere*, 2014, **101**, 21–27.
61 M. B. McBride and L. G. Wessellnk, *Environ. Sci. Technol.*, 1988, **22**, 703–708.
62 Y. H. Li, S. Wang, A. Cao, D. Zhao, X. Zhang, C. Xu, Z. Luan, D. Ruan, J. Liang, D. Wu and B. Wei, *Chem. Phys. Lett.*, 2001, **350**, 412–416.
63 L. Lv, J. He, M. Wei, D. Evans and Z. Zhou, *Water Res.*, 2007, **41**, 1534–1542.
64 S. Jagtap, M. K. N. Yenkie, N. Labhsetwar and S. Rayalu, *Microporous Mesoporous Mater.*, 2011, **142**, 454–463.
65 H. Cai, G. Chen, C. Peng, L. Xu, X. Zhu, Z. Zhang, Y. Dong, G. Shang, F. Ke, H. Gao and X. Wan, *RSC Adv.*, 2015, **5**, 29266–29275.
66 H. M. Cai, G. J. Chen, C. Y. Peng, Z. Z. Zhang, Y. Y. Dong, G. Z. Shang, X. H. Zhu, H. J. Gao and X. C. Wan, *Appl. Surf. Sci.*, 2015, **328**, 34–44.
67 J. Zhu, X. Lin, P. Wu, Q. Zhou and X. Luo, *Appl. Surf. Sci.*, 2015, **357**, 91–100.
68 M. Mohapatra, K. Rout, P. Singh, S. Anand, S. Layek, H. C. Verma and B. K. Mishra, *J. Hazard. Mater.*, 2011, **186**, 1751–1757.
69 N. A. Medellin-Castillo, R. Leyva-Ramos, E. Padilla-Ortega, R. O. Perez, J. V. Flores-Cano and M. S. Berber-Mendoza, *J. Ind. Eng. Chem.*, 2014, **20**, 4014–4021.
70 Z. Jin, Y. Jia, T. Luo, L. T. Kong, B. Sun, W. Shen, F. L. Meng and J. H. Liu, *Appl. Surf. Sci.*, 2015, **357**, 1080–1088.
71 S. Dong and Y. Wang, *Water Res.*, 2016, **88**, 852–860.
72 K. Y. A. Lin, Y. T. Liu and S. Y. Chen, *J. Colloid Interface Sci.*, 2016, **461**, 79–87.

